

# Enhancing the Sensitivity of Atom-Based Microwave-Field Electrometry Using a Mach-Zehnder Interferometer

Wenguang Yang,<sup>1,2</sup> Minyong Jing,<sup>1,2</sup> Hao Zhang,<sup>1,2,\*</sup> Linjie Zhang<sup>①</sup>,<sup>1,2,†</sup> Liantuan Xiao,<sup>1,2</sup> and Suotang Jia<sup>1,2</sup>

<sup>1</sup>*State Key Laboratory of Quantum Optics and Quantum Optics Devices, Institute of Laser Spectroscopy, Shanxi University, Taiyuan, 030006 Shanxi, People's Republic of China*

<sup>2</sup>*Collaborative Innovation Center of Extreme Optics, Shanxi University, Taiyuan, 030006 Shanxi, People's Republic of China*

 (Received 29 October 2022; revised 18 April 2023; accepted 9 May 2023; published 7 June 2023; corrected 6 July 2023)

We demonstrate the sensitivity enhancement of measurement of microwave electric fields by use of the full information of the complex atomic susceptibility. The transfer characteristics of both the microwave electric fields and the noise relevant to atoms, which are mapped to two quadrature components of the probe light, are systematically measured with use of a Mach-Zehnder interferometer. On the basis of the readout of the full complex atomic susceptibility, a sensitivity enhancement of 12 dB is achieved when the probe light has red detuning of 6 MHz. The results shed light on increasing the sensitivity of atomic sensors of microwave electric fields that is beyond the capability of the traditional antenna.

DOI: [10.1103/PhysRevApplied.19.064021](https://doi.org/10.1103/PhysRevApplied.19.064021)

## I. INTRODUCTION

An increasing number of researchers have moved toward the goal of sensing of microwave (MW) electric fields with Rydberg atoms because the exaggerated electrical characteristics of atoms are advantageous for high-sensitivity measurement. Many interesting studies have been conducted in recent years, including the some researches on accuracy [1], the first demonstration of vector microwave electrometry [2], related studies to increase sensitivity [3,4], and measurement of the frequency [5–7] and the phase [7,8] of MW electric fields. In particular, we reported an atomic superheterodyne that can be used to measure the amplitude of MW electric fields with a significant increase of sensitivity [7].

The research studies mentioned above focused on the imaginary part of the complex atomic susceptibility via direct optical readout. The predominant limit to the sensitivity is the noise in a laser, which consists of technical noise and shot noise from the photons, especially the noise induced by atomic ensembles. The influence of laser technical noise can be eliminated or reduced; for example, the fluctuation of laser power can be suppressed by balanced detection, the phase noise of the laser can be suppressed by lock the laser frequency to the frequency reference provided by a Fabry-Perot cavity made of ultralow-expansion glass as a stable frequency reference [9], and the noise of

photodetectors and the spectrum analyzer is much lower than that of optical-readout noise and is therefore ignored. However, the optical-readout noise from phase-noise-to-amplitude-noise (PN-to-AN) conversion through atomic ensembles cannot be eliminated. Previous work in the context of delayed light in electromagnetically induced transparency (EIT) [10] and magnetometers [11] investigated the noise spectrum with PN-to-AN conversion. In Rydberg-atom EIT systems, He *et al.* [12] experimentally demonstrated that the noise due to PN-to-AN conversion is suppressed on two-photon resonance. These research studies also concerned only the imaginary part of the complex atomic susceptibility, while only the PN-to-AN conversion process has been investigated. For the Mach-Zehnder-interferometer (MZI) measuring scheme, one can extract the real part of the atomic susceptibility for the study of magnetometer sensitivity [13] or the imaginary part for the study of the MW-electric-field sensitivity [3]. But more than that, it can be used to extract both the real and the imaginary part when the PN-to-AN conversion process is quantified in the measurement of MW electric fields based on Rydberg EIT.

To obtain the optimal sensitivity or signal-to-noise ratio (SNR), it is therefore important to analyze the main source of noise in the optical-readout process for measurement of MW electric fields. Unlike the sensitivity-enhancement scheme in Refs. [7,14], where an enhanced transduction parameter  $\gamma$  [15] is used, we focus on achieving the optimum condition for minimizing the output noise in a realistic Rydberg EIT scheme. The MW electric fields

\*haozhang@sxu.edu.cn

†zlj@sxu.edu.cn

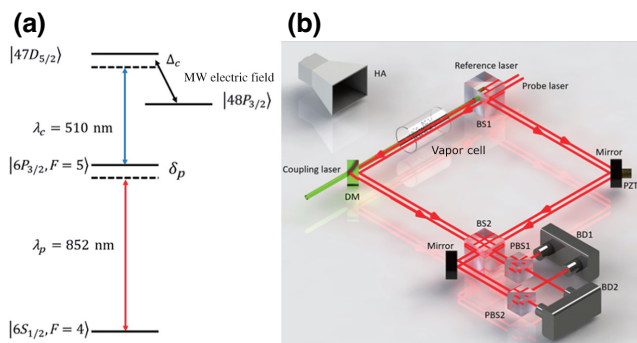


FIG. 1. (a) Energy-level diagram. The 852-nm and 510-nm lasers are the EIT probe laser and the coupling laser, respectively. The MW electric field couples to the  $47D_{5/2} \rightarrow 48P_{3/2}$  transition.  $\delta_p$  is the one-photon detuning and  $\Delta_c$  is the two-photon detuning. (b) Experimental setup. A free-space MZI containing a vapor cell with Cs atoms at room temperature. The transmission of the probe beam through the cell is monitored by a balanced detector (BD). BS, nonpolarizing beam splitter; DM, dichroic mirror; HA, horn antenna, OSC, oscilloscope; PBS, polarizing beam splitter; PZT, piezoelectric transducer.

can change the absorption and dispersion of the probe light, which is also the basic principle of measurement of microwave-field strength based on the EIT effect. In this paper, we report the measurement of the full information of the atomic susceptibility, namely, the real and imaginary parts, to enhance the sensitivity of MW electric fields based on EIT. Using the MZI, we record the optical-readout-noise power spectrum at the optimum biasing phase by adjusting the optical-path difference of the two arms of the MZI. Therefore, we present clear evidence to understand the degree of PN-to-AN conversion, and the experimental results show that the optimum condition for maximizing the SNR in a realistic Rydberg-atom EIT scheme can be achieved by adjustment of the one-photon detuning in the MZI. The one-photon detuning corresponding to the optimum sensitivity is  $-6$  MHz and the sensitivity is enhanced by 12 dB.

## II. EXPERIMENTAL SETUP

A four-level atom system is formed by a ground state  $|1\rangle$ ,  $6S_{1/2}(F=4)$ , an intermediate state  $|2\rangle$ ,  $6P_{3/2}(F'=5)$ , and two adjacent Rydberg states  $|3\rangle$  and  $|4\rangle$ ,  $47D_{5/2}$  and  $48P_{3/2}$  [see Fig. 1(a)]. The model is used to provide an explanation for the experimental observations. The probe laser drives the  $6S_{1/2}(F=4) \rightarrow 6P_{3/2}(F'=5)$  transition at 852 nm, and the beam from the coupling laser resonant with the Cs  $6P_{3/2}(F'=5) \rightarrow 47D_{5/2}$  transition at 510 nm is counterpropagating in the vapor cell.  $\delta_p$  is the one-photon detuning and  $\Delta_c$  is the two-photon detuning. Both lasers are locked to an ultrastable Fabry-Perot cavity with a linewidth of about 10 Hz and noise suppression of 70 dB [9].

Figure 1(b) shows the experimental setup. The probe light is divided into two beams (the detection beam and the reference beam) with orthogonal polarization directions by a polarization beam splitter. The detection beam and the reference beam are divided into two beams by a nonpolarizing beam splitter (BS1). These two components travel along different paths and then are recombined by a second nonpolarizing beam splitter (BS2). They form two typical free-space MZIs. The aim of the reference MZI is to lock the phase and the other MZI is used to sense the phase variation. Spectral information on the phase difference  $\Delta\phi$  between the two optical paths of the interferometer can be monitored through the digital oscilloscope. A cylindrical vapor cell filled with cesium atoms is located in the signal arm of the MZI. The probe laser has a power of  $20 \mu\text{W}$  and a waist diameter of  $800 \mu\text{m}$ , and the coupling laser has a power of 50 mW and a waist diameter of 1 mm. The amplitude-modulated MW electric field (6.94 GHz) is led into the vapor cell by a horn antenna, and couples resonantly to the  $47D_{5/2} \rightarrow 48P_{3/2}$  transition. The modulated optical signal carrying intensity information on the MW electric field is fed into the spectrum analyzer. The frequency of the modulated signal is 150 kHz. The resolution bandwidth and the video bandwidth are both 1 kHz. The EIT transmission signal can also be analyzed with an oscilloscope.

Using the MZI, we precisely measure the complex susceptibility, which comprises both the phase and the absorption of probe light due to the coherence effect induced by the interaction of the probe light, the coupling light, and the modulated MW electric field among the four-level atom system.

## III. RESULTS AND DISCUSSION

To fully understand the PN-to-AN conversion process in Rydberg EIT, we first measure the EIT transmission spectrum with the oscilloscope along with the intensity-noise spectrum (INS) of the optical readout with the spectrum analyzer. Figure 2 shows the transmission signal and the INS versus the coupling-laser frequency detuning. The INS is recorded directly by a single photodiode and a spectrum analyzer operating in zero-span mode, so the transmission signal and the INS can be obtained synchronously. The analysis frequency is 150 kHz, at which the lowest noise is obtained when the laser weakly interacts with the atoms. Figure 2(a) indicates that the INS strongly depends on the coupling-laser frequency (i.e., two-photon detuning) in the EIT transmission window, and the noise is suppressed at the two-photon resonance and is about 8 dB lower than in the off-two-photon-resonance case. Similar results were reported in Ref. [12], but our results show the noise on both sides of the resonance is asymmetrical. The phenomenon was reasonably explained by the atomic noise in the red-detuning condition being

less than the noise in the resonant and blue-detuning condition in Ref. [10]. It is important to point out that the intensity noise within the EIT linewidth critically comes from PN-to-AN conversion due to interaction between the atoms and the laser rather than the shot noise of the laser. Figure 2(b) shows the transmission signal and the INS with an amplitude-modulated MW electric field of about 3 mV/cm, which is calibrated by the EIT Autler-Townes-splitting effect. The modulation depth of 1% associated with the MW-electric-field strength to be measured is too small to change the EIT Autler-Townes splitting. The noise in the transmission window is suppressed once more, and the asymmetry of noise power still exists. The INS power when the coupling-laser frequency is blue detuned is lower than that for red detuning. For the direct measurement scheme, the magnitude of the transmission can be used to infer the amplitude-modulated MW electric field led into the vapor cell, but only with regard to the imaginary part of the atomic susceptibility [16]. In addition, more participating atoms can be maintained at two-photon resonance than in the off-two-photon-resonance case.

The MZI is the prototypical apparatus used in ultraprecise interferometric measurements [17–22]. In a classical MZI, one of the inputs is placed in a coherent state, whereas the other is not excited. In this case the phase sensitivity is bounded by the shot-noise limit of photons, which is due to quantum fluctuations at the unused port. A magnetometer based on atomic coherence effects was analyzed by Fleischhauer and Scully [23] using a quantum Langevin approach, and theoretically they determined the quantum noise limits for the phase-shift measurement in the MZI by taking into account the pump-laser fluctuations and Doppler broadening. An MZI offers the possibility that not only both the real part and the imaginary part of the

atomic susceptibility can be measured but also that the PN-to-AN conversion process can be quantified.

In our experiments, the optical-readout signal of the MZI is given by

$$I = a \cos(\Delta\phi) = a \cos(\Delta\phi' + \Delta\phi). \quad (1)$$

The parameter  $a$  is the transmission loss and  $\Delta\phi'$  is the phase shift induced by the MW electric field:

$$a \propto \exp\left\{\frac{-2\pi l \text{Im}[\chi(\delta_p, \Omega_{\text{MW}})]}{\lambda_p}\right\}, \quad (2)$$

$$\Delta\phi' \propto \frac{\pi \text{Re}[\chi(\delta_p, \Omega_{\text{MW}})]}{\lambda_p}, \quad (3)$$

where  $l$  is the length of the cell,  $\lambda_p$  is the wavelength,  $\delta_p$  is the detuning of the probe laser,  $\Omega_{\text{MW}}$  is the Rabi frequency of the MW electric field, and  $\chi$  is the susceptibility, which we can obtain from a density-matrix analysis of the system [24–26].

Inspired by Refs. [10,11], we note that the noise from the PN-to-AN conversion of probe light cannot be ignored. The optical-readout signal and the noise are measured and the one-photon-detuning dependence of the SNR in the MZI is determined. In Fig. 3,  $\Delta_c + \delta_p$  is kept zero. Figs. 3(a)–3(c), 3(d)–3(f), and 3(g)–3(i) show the spectrum signal intensity at an analysis frequency of 150 kHz, the noise, and the SNR for  $\delta_p = 0$  [Figs. 3(a), 3(d), and 3(g)],  $\delta_p = -6$  MHz [Figs. 3(b), 3(e), and 3(h)], and  $\delta_p = 6$  MHz [Figs. 3(c), 3(f), and 3(i)] when the piezoelectric transducer is adjusted to change the phase difference between the two arms of the MZI from 0 to  $2\pi$ . The measured output-signal data and the theoretical simulation obtained

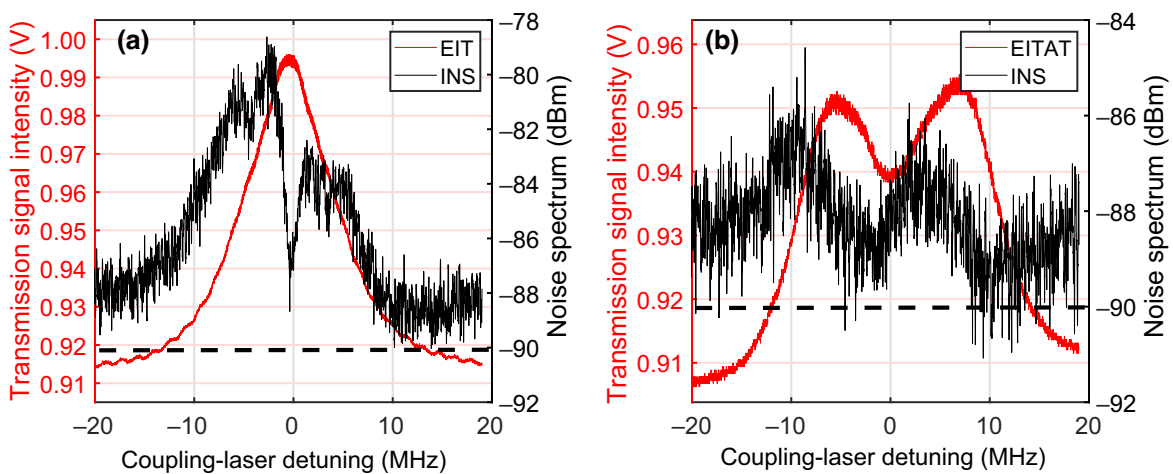


FIG. 2. Transmission signal and intensity-noise spectrum versus the coupling-laser frequency detuning. The red line is the transmission signal and the black line is the intensity-noise spectrum at an analysis frequency of 150 kHz. The spectrum when the MW electric field is turned off is shown in (a) and the spectrum when the MW electric field is turned on (about 3 mV/cm) is shown in (b). EITAT, EIT Autler-Townes splitting.

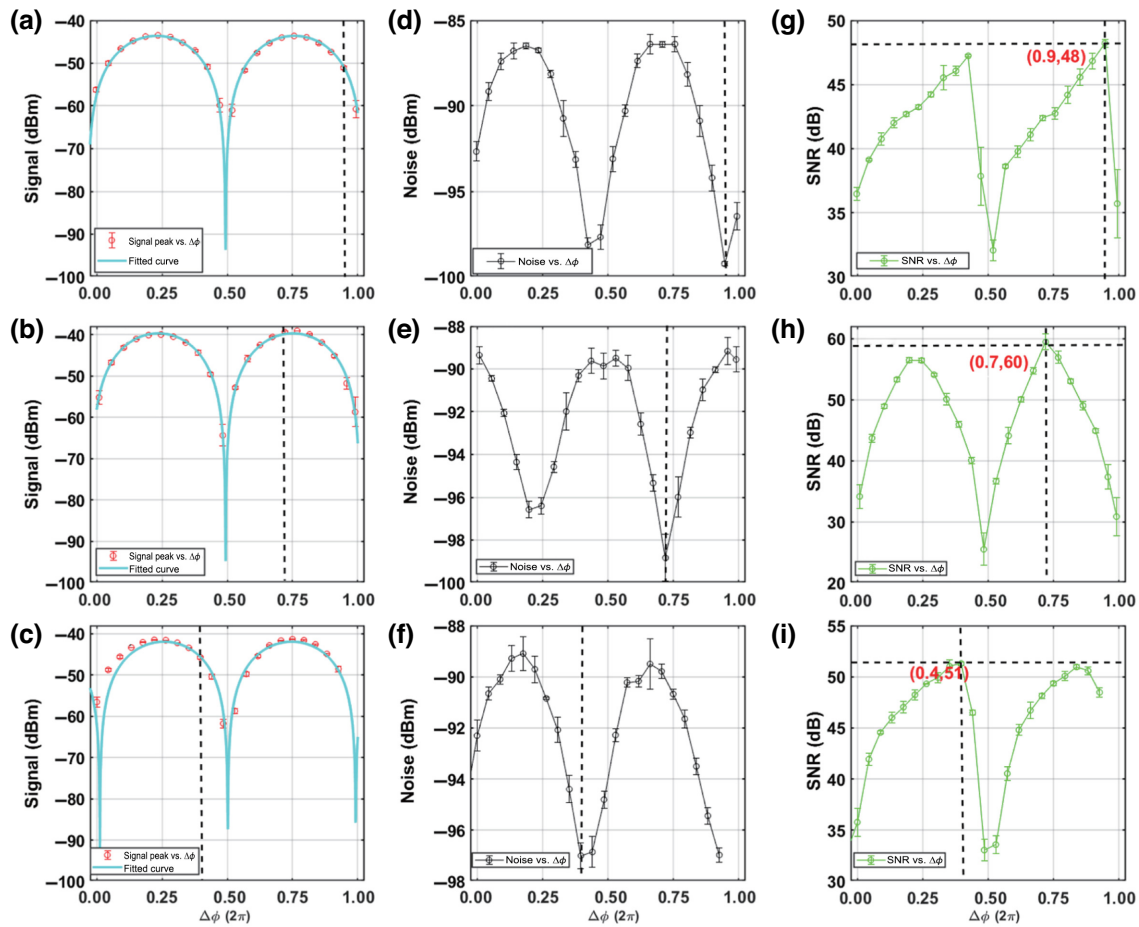


FIG. 3. Spectrum signal intensity and noise when the PZT is adjusted. In (a)–(c) the red circles are the peak values of the demodulated signal and the cyan curves are the fitted curves, in (d)–(f) the black circles are the noise, and in (g)–(i) the green lines are the SNR and the coordinates marked in red represent the location and the value of the optimum SNR. For (a),(d),(g),  $\delta_p = 0$ , for (b),(e),(h),  $\delta_p = -6$  MHz, and for (c),(f),(i),  $\delta_p = 6$  MHz.

with Eq. (1) with the optimum fitting parameters are shown in Figs. 3(a)–3(c). The mismatch between the experimental data and the fitted curve is attributed to nonlinear characteristics of the piezoelectric transducer. The maximum signal strength is almost always found in the quadrature phase for  $\delta_p = 0$  MHz,  $\delta_p = -6$  MHz, and  $\delta_p = 6$  MHz as shown in Figs. 3(a)–3(c), but the variation of noise is different, as shown in Figs. 3(d)–3(f). The dependencies of the signal versus the relative phase are insensitive to detuning of the probe laser, while the relationship between noise power and relative phase varies dramatically due to the different PN-to-AN conversion efficiency, which leads to distinctive SNR behavior versus the relative phase at a certain detuning of the probe laser. Figures 3(g)–3(i) show that the optimum SNR is not exactly present in the quadrature amplitude or quadrature phase. This result is attributed to the fact that we can quantify the PN-to-AN conversion process with the MZI. The Rydberg atoms prepared with coupling (probe) light red (blue) detuned experience an attractive potential  $47D_{5/2}-47D_{5/2}$ , leading to higher

collisional and ionization rates compared with those in the coupling-light (probe-light) blue-detuning (red-tuning) condition, and this produces stronger background electric fields in the vapor cell and reduces the number of effective atoms [27,28]. The stronger background electric fields in the vapor cell lead to the energy shift of the Rydberg level. This energy shift breaks the EIT (i.e., two-photon-resonance) condition, which increases the efficiency of PN-to-AN conversion.

In Fig. 4, the results show the optimum SNR is at  $\delta_p = -6$  MHz and the SNR is increased by 12 dB in comparison with the on-resonance case. We obtain the minimum detectable field  $E_{\min}$  in a measurement time of 1 s and derive a sensitivity of  $1.3 \mu\text{V} \cdot \text{cm}^{-1} \cdot \text{Hz}^{-1/2}$ . Without introducing a transduction parameter, we increase the sensitivity by a factor of 5 compared with the work reported in Ref. [3]. In addition, as shown in Fig. 2, the PN-to-AN conversion process, with an MW electric field of 3 mV/cm, which is the same value as the optimized local MW electric field in the atomic superheterodyne

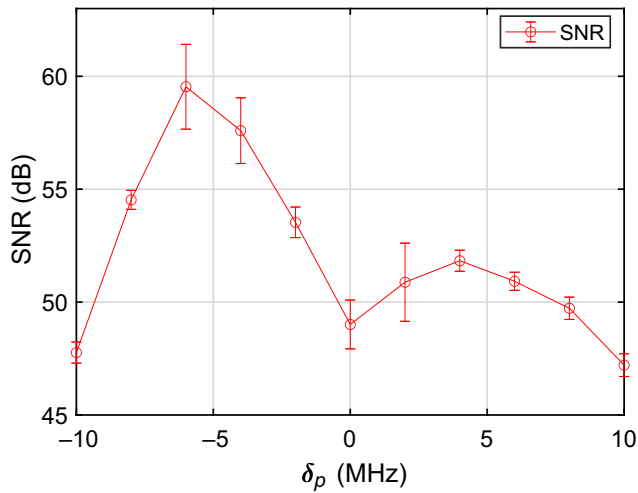


FIG. 4. Output SNR of the MZI as a function of the one-photon detuning  $\delta_\rho$ . Here the SNR is extracted from the optimum phase-measurement points shown in Figs. 3(g)–3(i). The results show the SNR is increased by 12 dB when the probe-light frequency is red detuned by 6 MHz from resonance.

scheme, does not change compared with the direct detection. Optimizing single-photon detuning does not result in the least-noisy measurement position. Compared with the atomic superheterodyne scheme, a less-local oscillator is used in our measurements. Therefore, on the basis of the superheterodyne scheme, the MZI scheme will be a supplement to increase the sensitivity. We expect to achieve the same SNR increase of 12 dB, corresponding to a sensitivity of  $13 \text{ nV} \cdot \text{cm}^{-1} \cdot \text{Hz}^{-1/2}$ .

The sensitivity benchmark is that of an ideal quantum sensor operating at the standard quantum limit  $\mathcal{S} = h/u\sqrt{T_2TN}$  [29], which shows the sensitivity of the MW-electric-field strength is crucially dependent on the number of atoms participating in the measurement  $N$ , the measurement time  $T$ , and the atom relaxation time  $T_2$ . In a realistic Rydberg-atom EIT scheme, the PN-to-AN conversion via absorption and dispersion effects is also critical in determining the sensitivity. The experimental results show that the output noise of the MZI is sensitive to one-photon frequency detuning.

#### IV. CONCLUSION

In this work, we investigate the complex atomic susceptibility, and the measurement scheme using an MZI realizes joint measurement of the quadrature components of the output signal. The experimental results show that the PN-to-AN conversion depends not only on the two-photon detuning but also on the one-photon detuning in the EIT window. We conclude that the optimum SNR is at one-photon detuning of  $-6$  MHz and is increased by 12 dB. The present results may have practical significance for achieving standard quantum limit sensitivity

of atom-based microwave-field electrometry with realistic lasers.

#### ACKNOWLEDGMENTS

This work was supported by the National Key R&D Program of China (Grant No. 2022YFA1404003), the National Natural Science Foundation of China (Grants No. 61827824 and No. 61975104), the Innovation Program for Quantum Science and Technology (Grant No. 2021ZD0302100), the Fund for Science and Technology on Electronic Information Control Laboratory, and the Fund for Shanxi ‘1331 Project’ Key Subjects Construction, Bairen Project of Shanxi Province, China.

- [1] H. Fan, S. Kumar, J. Sheng, J. P. Shaffer, C. L. Holloway, and J. A. Gordon, Effect of Vapor-Cell Geometry on Rydberg-Atom-Based Measurements of Radio-Frequency Electric Fields, *Phys. Rev. Appl.* **4**, 044015 (2015).
- [2] J. Sedlacek, A. Schwettmann, H. Kübler, and J. Shaffer, Atom-Based Vector Microwave Electrometry Using Rubidium Rydberg Atoms in a Vapor Cell, *Phys. Rev. Lett.* **111**, 063001 (2013).
- [3] S. Kumar, H. Fan, H. Kübler, J. Sheng, and J. P. Shaffer, Ror2 signaling regulates Golgi structure and transport through IFT20 for tumor invasiveness, *Sci. Rep.* **7**, 1 (2017).
- [4] J. A. Sedlacek, A. Schwettmann, H. Kübler, R. Löw, T. Pfau, and J. P. Shaffer, Microwave electrometry with Rydberg atoms in a vapour cell using bright atomic resonances, *Nat. Phys.* **8**, 819 (2012).
- [5] M. T. Simons, J. A. Gordon, C. L. Holloway, D. A. Anderson, S. A. Miller, and G. Raithel, Using frequency detuning to improve the sensitivity of electric field measurements via electromagnetically induced transparency and Autler-Townes splitting in Rydberg atoms, *Appl. Phys. Lett.* **108**, 174101 (2016).
- [6] J. A. Gordon, M. T. Simons, A. H. Haddab, and C. L. Holloway, Weak electric-field detection with sub-1 Hz resolution at radio frequencies using a Rydberg atom-based mixer, *AIP Adv.* **9**, 045030 (2019).
- [7] M. Jing, Y. Hu, J. Ma, H. Zhang, L. Zhang, L. Xiao, and S. Jia, Atomic superheterodyne receiver based on microwave-dressed Rydberg spectroscopy, *Nat. Phys.* **16**, 911 (2020).
- [8] M. T. Simons, A. H. Haddab, J. A. Gordon, and C. L. Holloway, A Rydberg atom-based mixer: Measuring the phase of a radio frequency wave, *Appl. Phys. Lett.* **114**, 114101 (2019).
- [9] M. Jing, P. Zhang, S. Yuan, L. Zhang, L. Xiao, and S. Jia, High bandwidth laser frequency locking for wideband noise suppression, *Opt. Exp.* **29**, 7916 (2021).
- [10] J. Zhang, J. Cai, Y. Bai, J. Gao, and S.-Y. Zhu, Optimization of the noise property of delayed light in electromagnetically induced transparency, *Phys. Rev. A* **76**, 033814 (2007).
- [11] Y. Xiao, T. Wang, M. Baryakhtar, M. Van Camp, M. Crescimanno, M. Hohensee, L. Jiang, D. F. Phillips, M. D. Lukin, and S. F. Yelin, *et al.*, Electromagnetically induced

- transparency with noisy lasers, *Phys. Rev. A* **80**, 041805 (2009).
- [12] J. He, Q. Liu, Z. Yang, Q. Niu, X. Ban, and J. Wang, Noise spectroscopy with a Rydberg ensemble in a hot atomic vapor cell, *Phys. Rev. A* **104**, 063120 (2021).
- [13] M. O. Scully and M. Fleischhauer, High-Sensitivity Magnetometer Based on Index-Enhanced Media, *Phys. Rev. Lett.* **69**, 1360 (1992).
- [14] D.-S. Ding, Z.-K. Liu, B.-S. Shi, G.-C. Guo, K. Mølmer, and C. S. Adams, Enhanced metrology at the critical point of a many-body Rydberg atomic system, *Nat. Phys.* **18**, 1447 (2022).
- [15] C. L. Degen, F. Reinhard, and P. Cappellaro, Quantum sensing, *Rev. Mod. Phys.* **89**, 035002 (2017).
- [16] S. Kumar, H. Fan, H. Kübler, A. J. Jahangiri, and J. P. Shaffer, Rydberg-atom based radio-frequency electrometry using frequency modulation spectroscopy in room temperature vapor cells, *Opt. Exp.* **25**, 8625 (2017).
- [17] S. A. Aljunid, M. K. Tey, B. Chng, T. Liew, G. Maslennikov, V. Scarani, and C. Kurtsiefer, Phase Shift of a Weak Coherent Beam Induced by a Single Atom, *Phys. Rev. Lett.* **103**, 153601 (2009).
- [18] M. A. Armen, J. K. Au, J. K. Stockton, A. C. Doherty, and H. Mabuchi, Adaptive Homodyne Measurement of Optical Phase, *Phys. Rev. Lett.* **89**, 133602 (2002).
- [19] W. D. Oliver, Y. Yu, J. C. Lee, K. K. Berggren, L. S. Levitov, and T. P. Orlando, Mach-Zehnder interferometry in a strongly driven superconducting qubit, *Science* **310**, 1653 (2005).
- [20] J. G. Rarity, P. R. Tapster, E. Jakeman, T. Larchuk, R. A. Campos, M. C. Teich, and B. E. Saleh, Two-Photon Interference in a Mach-Zehnder Interferometer, *Phys. Rev. Lett.* **65**, 1348 (1990).
- [21] M. O. Scully and M. Fleischhauer, High-Sensitivity Magnetometer Based on Index-Enhanced Media, *Phys. Rev. Lett.* **69**, 1360 (1992).
- [22] M. Xiao, Y. Li, S. Jin, and J. Gea-Banaclache, Measurement of Dispersive Properties of Electromagnetically Induced Transparency in Rubidium Atoms, *Phys. Rev. Lett.* **74**, 666 (1995).
- [23] M. Fleischhauer and M. O. Scully, Quantum sensitivity limits of an optical magnetometer based on atomic phase coherence, *Phys. Rev. A* **49**, 1973 (1994).
- [24] G. Vemuri, G. Agarwal, and B. N. Rao, Sub-Doppler resolution in inhomogeneously broadened media using intense control fields, *Phys. Rev. A* **53**, 2842 (1996).
- [25] Y. Rostovtsev, I. Protsenko, H. Lee, and A. Javan, From laser-induced line narrowing to electromagnetically induced transparency in a Doppler-broadened system, *J. Mod. Opt.* **49**, 2501 (2002).
- [26] M. Pack, R. Camacho, and J. Howell, Electromagnetically induced transparency line shapes for large probe fields and optically thick media, *Phys. Rev. A* **76**, 013801 (2007).
- [27] S. M. Bohaichuk, D. Booth, K. Nickerson, H. Tai, and J. P. Shaffer, Origins of Rydberg-Atom Electrometer Transient Response and Its Impact on Radio-Frequency Pulse Sensing, *Phys. Rev. Appl.* **18**, 034030 (2022).
- [28] T. Amthor, M. Reetz-Lamour, S. Westermann, J. Denkskat, and M. Weidemüller, Mechanical Effect of van der Waals Interactions Observed in Real Time in an Ultracold Rydberg Gas, *Phys. Rev. Lett.* **98**, 023004 (2007).
- [29] J. Kitching, S. Knappe, and E. A. Donley, Atomic sensors – a Review, *IEEE Sens. J.* **11**, 1749 (2011).

*Correction:* An error in the presentation of the units given in the caption of Figure 3 has been set right. The unit given in the second sentence of the fifth paragraph in Sec. III contained an error and has been fixed.